14th World Congress on Computational Mechanics (WCCM)
ECCOMAS Congress 2020
Virtual Congress: 11-15 January 2021
F. Chinesta, R. Abgrall, O. Allix and M. Kaliske (Eds)

ON A PROPER TENSORIAL SUBGRID HEAT FLUX MODEL

F.X. Trias[1], F. Dabbagh[2], D. Santos[1], A. Gorobets[3], A. Oliva[1]

[1] Heat and Mass Transfer Technological Center,
Technical University of Catalonia, C/Colom 11, 08222 Terrassa (Barcelona)
{francesc.xavier.trias,daniel.santos.serrano,asensio.oliva}@upc.edu

[2] Christian Doppler Laboratory for Multi-Scale Modeling of Multiphase Processes,
Johannes Kepler University, Altenbergerstraße 69, 4040 Linz, Austria. firas.dabbagh@jku.at

[3] Keldysh Institute of Applied Mathematics, 4A, Miusskaya Sq., Moscow 125047, Russia.
andrey.gorobets@gmail.com

Key words: LES, SGS models, buoyancy-driven flows, turbulence

Abstract. In this work, we aim to shed light to the following research question: *can we find a nonlinear tensorial subgrid-scale (SGS) heat flux model with good physical and numerical properties, such that we can obtain satisfactory predictions for buoyancy-driven turbulent flows?* This is motivated by our findings showing that the classical (linear) eddy-diffusivity assumption, $q^{eddy} \propto \nabla\overline{T}$, fails to provide a reasonable approximation for the actual SGS heat flux, $q = \overline{uT} - \overline{u}\,\overline{T}$: namely, *a priori* analysis for air-filled Rayleigh-Bénard convection (RBC) clearly shows a strong misalignment. In the quest for more accurate models, we firstly study and confirm the suitability of the eddy-viscosity assumption for RBC carrying out *a posteriori* tests for different models at very low Prandtl numbers (liquid sodium, $Pr = 0.005$) where no heat flux SGS activity is expected. Then, different (nonlinear) tensor-diffusivity SGS heat flux models are studied *a priori* using DNS data of an air-filled ($Pr = 0.7$) RBC at Rayleigh numbers up to 10^{11}. Apart from having good alignment trends with the actual SGS heat flux, we also restrict ourselves to models that are numerically stable *per se* and have the proper cubic near-wall behavior. This analysis leads to a new family of SGS heat flux models based on the symmetric positive semi-definite tensor $\mathsf{G}\mathsf{G}^T$ where $\mathsf{G} \equiv \nabla\overline{u}$, *i.e.* $q \propto \mathsf{G}\mathsf{G}^T\nabla\overline{T}$, and the invariants of the $\mathsf{G}\mathsf{G}^T$ tensor. Finally, relevant numerical aspects regarding the implementation of this type of models are discussed in detail. A list of physical and numerical properties is identified and subsequently imposed, leading to a symmetry-preserving discretization that is based on discrete operators already available in any CFD code.

1 INTRODUCTION

In this work, we plan to shed light on the following research question: *can we find a nonlinear subgrid-scale (SGS) heat flux model with good physical and numerical properties, such that we can obtain satisfactory predictions for buoyancy driven turbulent flows?* This is motivated by our findings showing that the classical (linear) eddy-diffusivity assumption fails to provide a reasonable approximation for the SGS heat flux. This was shown in a previous work [1] where SGS features were studied *a priori* for a Rayleigh-Bénard convection (RBC). We also concluded that only nonlinear (or tensorial) models can

give good approximations of the actual SGS heat flux. Briefly, large-eddy simulation (LES) equations arise from applying a spatial commutative filter, with filter length δ, to the incompressible Navier-Stokes and thermal energy equations,

$$\partial_t \overline{u} + (\overline{u}\cdot\nabla)\overline{u} = (Pr/Ra)^{1/2}\ \nabla^2\overline{u} - \nabla\overline{p} + \overline{f} - \nabla\cdot\tau, \tag{1}$$

$$\partial_t \overline{T} + (\overline{u}\cdot\nabla)\overline{T} = (Ra/Pr)^{-1/2}\nabla^2\overline{T} \qquad\qquad - \nabla\cdot q, \tag{2}$$

where $\overline{u}$, $\overline{T}$ and $\overline{p}$ are respectively the filtered velocity, temperature and pressure, and the incompressibility constraint reads $\nabla\cdot\overline{u}=0$. The SGS stress tensor, $\tau = \overline{u\otimes u} - \overline{u}\otimes\overline{u}$, and the SGS heat flux vector, $q = \overline{uT} - \overline{u}\,\overline{T}$, represent the effect of the unresolved scales, and they need to be modeled in order to close the system. The most popular approach is the eddy-viscosity assumption, where the SGS stress tensor is assumed to be aligned with the local rate-of-strain tensor, $\mathsf{S} = 1/2(\nabla\overline{u} + \nabla\overline{u}^t)$, *i.e.* $\tau \approx -2\nu_e \mathsf{S}(\overline{u})$. By analogy, the SGS heat flux, q, is usually approximated using the gradient-diffusion hypothesis (linear modeling), given by

$$q \approx -\kappa_t \nabla\overline{T} \qquad (\equiv q^{eddy}). \tag{3}$$

Then, the Reynolds analogy assumption is applied to evaluate the eddy-diffusivity, κ_t, via a constant turbulent Prandtl number, Pr_t, *i.e.* $\kappa_t = \nu_e/Pr_t$. These assumptions have been shown to be erroneous to provide accurate predictions of the SGS heat flux [1, 2, 3]. Namely, *a priori* analysis showed that the eddy-diffusivity assumption, q^{eddy} (Eq. 3), is completely misaligned with the actual subgrid heat flux, q (see Figure 1, left). In contrast, the tensor diffusivity (nonlinear) Leonard model [4], which is obtained by taking the leading term of the Taylor series expansion of q,

$$q \approx \frac{\delta^2}{12}\mathsf{G}\nabla\overline{T} \qquad (\equiv q^{nl}), \tag{4}$$

provides a much more accurate *a priori* representation of q (see Figure 1, left). Here, $\mathsf{G}\equiv\nabla\overline{u}$ represents the gradient of the resolved velocity field. It can be argued that the rotational geometries are prevalent in the bulk region over the strain slots, *i.e.* $|\Omega| > |\mathsf{S}|$ (see Refs [1, 5]). Then, the dominant anti-symmetric tensor, $\Omega = 1/2(\mathsf{G}-\mathsf{G}^T)$, rotates the thermal gradient vector, $\nabla\overline{T}$, to be almost perpendicular to q^{nl} (see Eq.4). Hence, the eddy-diffusivity paradigm is only valid in the not-so-frequent strain-dominated areas.

2 NONLINEAR SGS HEAT FLUX MODELS FOR LARGE-EDDY SIMULATION

Since the eddy-diffusivity, q^{eddy}, cannot provide an accurate representation of the SGS heat flux, we turn our attention to nonlinear models. As mentioned above, the Leonard model [4] given in Eq.(4) can provide a very accurate *a priori* representation of the SGS heat flux (see Figure 1, left). However, the local dissipation (in the L2-norm sense) is proportional to $\nabla T\cdot\mathsf{G}\nabla T = \nabla T\cdot\mathsf{S}\nabla T + \nabla T\cdot\Omega\nabla T = \nabla T\cdot\mathsf{S}\nabla T$. Since the velocity field is divergence-free, $\lambda_1^{\mathsf{S}}+\lambda_2^{\mathsf{S}}+\lambda_3^{\mathsf{S}} = \nabla\cdot u = 0$, the eigenvalues of S can be ordered $\lambda_1^{\mathsf{S}} \geqslant \lambda_2^{\mathsf{S}} \geqslant \lambda_3^{\mathsf{S}}$ with $\lambda_1^{\mathsf{S}} \geqslant 0$ (extensive eigendirection) and $\lambda_3^{\mathsf{S}} \leqslant 0$ (compressive eigendirection), and λ_2^{S} is either positive or negative. Hence, the local dissipation introduced by the model can take negative values; therefore, the Leonard model cannot be used as a standalone SGS heat flux model, since it can produce a finite-time blow-up. Attempts to overcome these instability issues are the so-called mixed model [2], where the Leonard model is combined with an eddy-diffusivity model, or the regularization technique proposed in [8] that projects the Leonard model onto a tensor with no energy

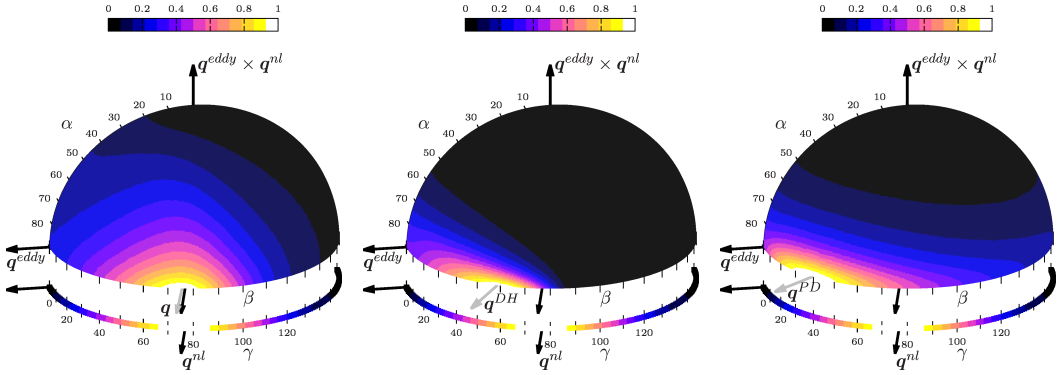

Figure 1: Joint probability distribution functions (PDF) of the angles (α,β) plotted on a half unit sphere to show the orientation in the space of the mixed model. From left to right, alignment trends of the actual SGS heat flux, q, the Daly and Harlow [6] model (Eq. 6) and the Peng and Davidson [7] model (Eq. 5). For simplicity, the JPDF and the PDF magnitudes are normalized by its maximal. For details the reader is referred to [1].

transfer in case of a negative dissipation event. Similar stability problems are encountered with the nonlinear tensorial model q^{PD} proposed by Peng and Davidson [7],

$$q \approx C_t \delta^2 \mathsf{S}\nabla\overline{T} \qquad (\equiv q^{PD}), \tag{5}$$

$$q \approx -\mathcal{T}_{SGS}\tau\nabla\overline{T} = -\frac{1}{|\mathsf{S}|}\frac{\delta^2}{12}\mathsf{G}\mathsf{G}^T\nabla\overline{T} \qquad (\equiv q^{DH}), \tag{6}$$

whereas the nonlinear model q^{DH} proposed by Daly and Harlow [6] relies on the positive semi-definite tensor $\mathsf{G}\mathsf{G}^T$. Here, $\mathcal{T}_{SGS} = 1/|\mathsf{S}|$ is the SGS timescale. Notice that the model proposed by Peng and Davidson, q^{PD}, can be viewed in the same framework if the SGS stress tensor is estimated by an eddy-viscosity model, *i.e.* $\tau \approx -2\nu_e\mathsf{S}$ and $\mathcal{T}_{SGS} \propto \delta^2/\nu_e$. These two models have shown a much better *a priori* alignment with the actual SGS heat flux, especially the DH model (see Figure 1, middle). Moreover, the DH is numerically stable since the tensor $\mathsf{G}\mathsf{G}^T$ is positive semi-definite. Hence, it seems appropriate to build models based on this tensor. However, the DH model does not have the proper near-wall behavior, *i.e.* $q \propto \langle v'T'\rangle = O(y^3)$ where y is the distance to the wall. An analysis of the DH model leads to $\mathsf{G}\mathsf{G}^T\nabla\overline{T} = O(y^1)$ [9]. Therefore, the near-wall cubic behavior is recovered if $\mathcal{T}_{SGS} \propto O(y^2)$. This is not the case of the timescale used in the Daly and Harlow [6] model, *i.e.* $\mathcal{T}_{SGS} = 1/|\mathsf{S}| = O(y^0)$.

At this point, it is interesting to observe that new timescales, $\mathcal{T}_{SGS}$, can be derived by imposing restrictions on the differential operators they are based on. For instance, let us consider models that are based on the principal invariants of the tensor $\mathsf{G}\mathsf{G}^T$

$$q \approx -C_M \left(P^p_{\mathsf{G}\mathsf{G}^T} Q^q_{\mathsf{G}\mathsf{G}^T} R^r_{\mathsf{G}\mathsf{G}^T}\right) \frac{\delta^2}{12}\mathsf{G}\mathsf{G}^T\nabla\overline{T} \qquad (\equiv q^{S2}), \tag{7}$$

where $P_{\mathsf{G}\mathsf{G}^T}$, $Q_{\mathsf{G}\mathsf{G}^T}$ and $R_{\mathsf{G}\mathsf{G}^T}$ are the first, second and third invariant of the $\mathsf{G}\mathsf{G}^T$ tensor. This tensor is proportional to the gradient model [11] given by the leading term of the Taylor series expansion of the subgrid stress tensor $\tau(\overline{u}) = (\delta^2/12)\mathsf{G}\mathsf{G}^T + O(\delta^4)$. Then, the exponents p, q and r in Eq.(7), must satisfy the following two equations

$$-6r-4q-2p = 1; \qquad 6r+2q = s, \tag{8}$$

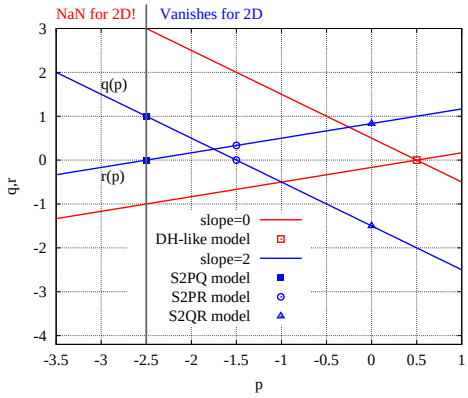

Figure 2: Solutions of the linear system of Eq.(8) for $s = 0$ (red lines) and $s = 2$ (blue lines). Each (r, p, q) represents a tensor-diffusivity model with the form of Eq.(7).

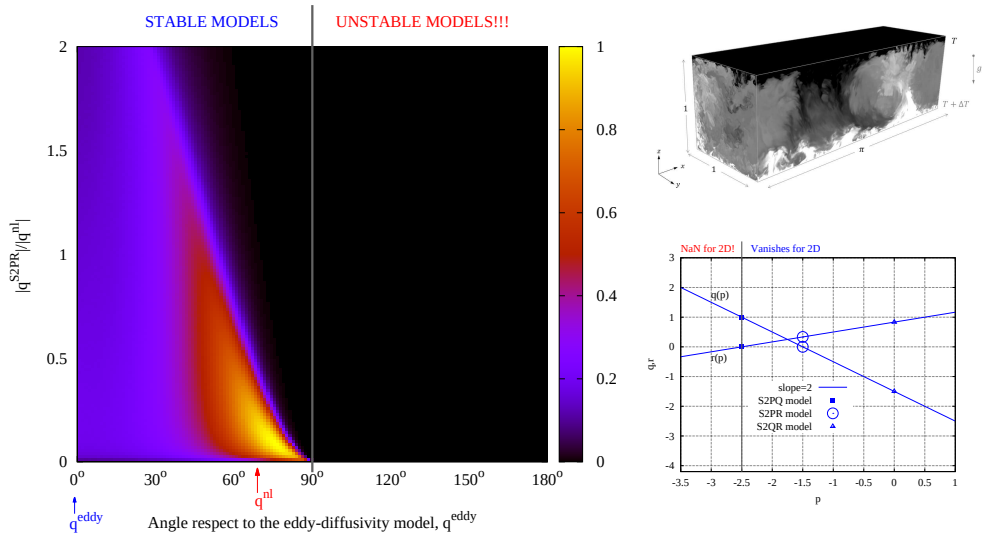

Figure 3: Joint PDF for the S2PR model (Eq. 10) in the space $(|q^{S2PR}|/|q^{nl}|, \beta)$ where the angle β is defined in Figure 1. The analyzed data corresponds to the bulk region of the air-filled Rayleigh-Bénard configuration at $Ra = 10^{11}$ studied in Ref. [10].

to guarantee that the differential operator has units of time, *i.e.* $[P^p_{\mathsf{GG}^T} Q^q_{\mathsf{GG}^T} R^r_{\mathsf{GG}^T}] = [T^1]$ and a slope s for the asymptotic near-wall behavior, *i.e.* $O(y^s)$. Solutions for $q(p,s) = -(1+s)/2 - p$ and $r(p,s) = (2s+1)/6 + p/3$ are displayed in Figure 2. If we restrict ourselves to solutions with the proper near-wall scaling, *i.e.* $s = 2$ (blue lines in Figure 2), a family of p-dependent models follows. Considering only

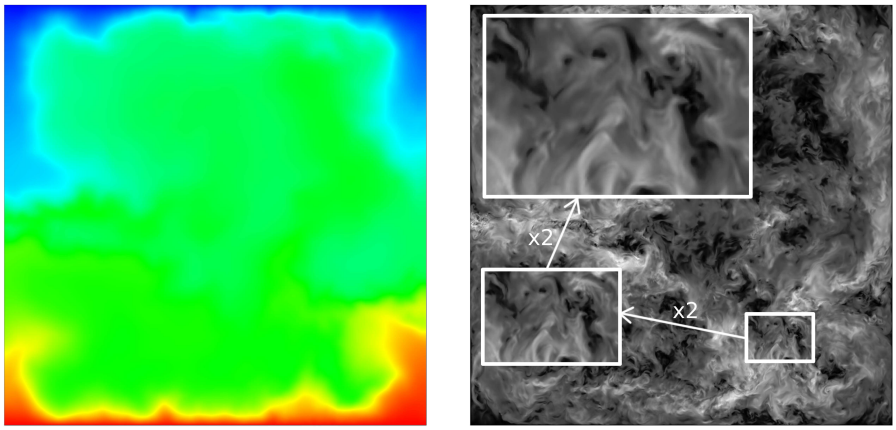

Figure 4: An instantaneous picture of the temperature field (left) and velocity magnitude (right), $|u|$, of the DNS simulation of RBC at $Ra = 7.14 \times 10^7$ and $Pr = 0.005$ (liquid sodium) carried out using a mesh of $966 \times 966 \times 2048 \approx 1911M$ grid points. See the movie in the database (http://www.cttc.upc.edu/downloads/RBC_lowPr).

solutions involving only two principal invariants of the tensor $\mathsf{G}\mathsf{G}^T$, three models follow

$$q^{S2PQ} = -C_{s2pq} P_{\mathsf{G}\mathsf{G}^T}^{-5/2} Q_{\mathsf{G}\mathsf{G}^T} \frac{\delta^2}{12} \mathsf{G}\mathsf{G}^T \nabla\overline{T}, \tag{9}$$

$$q^{S2PR} = -C_{s2pr} P_{\mathsf{G}\mathsf{G}^T}^{-3/2} R_{\mathsf{G}\mathsf{G}^T}^{1/3} \frac{\delta^2}{12} \mathsf{G}\mathsf{G}^T \nabla\overline{T}, \tag{10}$$

$$q^{S2QR} = -C_{s2qr} Q_{\mathsf{G}\mathsf{G}^T}^{3/2} R_{\mathsf{G}\mathsf{G}^T}^{5/6} \frac{\delta^2}{12} \mathsf{G}\mathsf{G}^T \nabla\overline{T}, \tag{11}$$

for $p = -5/2$, $p = -1.5$ and $p = 0$, respectively. These three solutions are represented in Figure 2. Apart from being unconditionally stable, these models display very good *a priori* alignment trends in the bulk (see Figure 3) similar to the PD model (see Figure 1, middle) but also in the near-wall region [9]. Hence, we consider that they are very good candidates for *a posteriori* LES of buoyancy-driven flows.

3 ASSESSMENT OF EDDY-VISCOSITY MODELS AT VERY LOW PRANDTL NUMBERS

At this stage, *a posteriori* results are necessary to assess the performance of the newly proposed SGS heat flux models. However, apart from the underlying numerics, such results will be strongly influenced by the SGS stress tensor model. Hence, we first aim to answer the following research question: *are eddy-viscosity models for momentum able to provide satisfactory results for turbulent Rayleigh-Bénard convection?* In order to shed light to this, a set of simulations at $Pr = 0.005$ (liquid sodium) have been carried out at $Ra = 7.14 \times 10^6$ and $Ra = 7.14 \times 10^7$. Figure 4 displays a snapshot of the temperature and velocity magnitude for the DNS simulation at the highest Ra. This clearly illustrates the separation between the smallest scales of temperature and velocity, *i.e.* the ratio between the Kolmogorov length scale and the Obukhov-Corrsin length scale is given by $Pr^{3/4}$ [12]. Therefore, for a $Pr = 0.005$ (liquid sodium) we have a separation of more than one decade. Hence, it is possible to combine an LES simulation for the velocity field with the numerical resolution of all the relevant scales of the thermal field. Regarding this, results shown in Figure 5 seem to confirm the adequacy of eddy-viscosity models for this kind of flows. Namely, Figure 5 (left) shows the Nusselt number for a set of meshes and eddy-viscosity

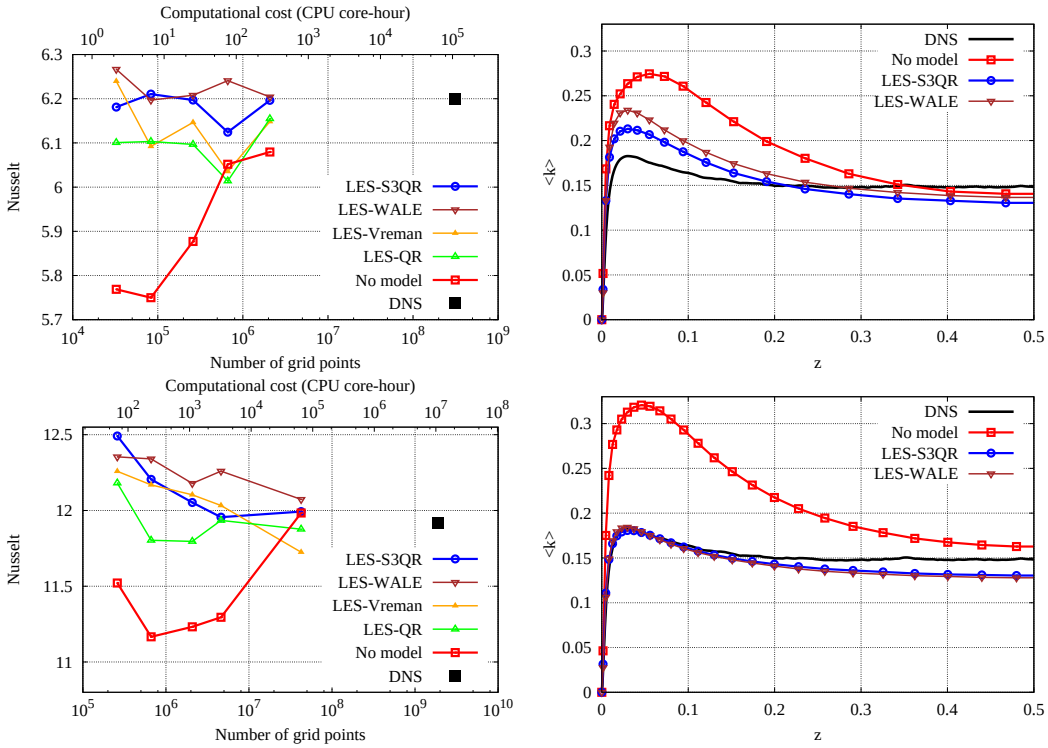

Figure 5: Comparison of LES (and no-model) versus DNS results of liquid-sodium ($Pr = 0.005$) RBC at $Ra = 7.14 \times 10^6$ and 7.14×10^7. Left: average Nusselt for different meshes at $Ra = 7.14 \times 10^6$ (top) and $Ra = 7.14 \times 10^7$ (bottom). Corresponding computational costs at the MareNostrum 4 supercomputer are shown in the top of the plots. Right: LES results of turbulent kinetic energy at cavity mid-width for a $64 \times 36 \times 36$ (top) and $96 \times 52 \times 52$ (bottom) meshes compared with the DNS results obtained with a mesh of $488 \times 488 \times 1280 \approx 305M$.

models: the WALE model [13], the Vreman model [14], the QR model [15] and the S3QR model [16]. Results obtained without SGS model are also shown to illustrate the effect of the eddy-viscosity models to improve the solution. At first sight it can be observed that, in general, all LES solutions are in rather good agreement with the DNS data even for the coarsest grids ($48 \times 26 \times 26$ for $Ra = 7.14 \times 10^6$ and $96 \times 52 \times 52$ for $Ra = 7.14 \times 10^7$ whereas only the finest ones ($128 \times 72 \times 72$ and $192 \times 104 \times 104$ at $Ra = 7.14 \times 10^6$ and $512 \times 288 \times 288$ at $Ra = 7.14 \times 10^7$) can provide accurate results when the model is switched off. A closer inspection shows that slightly better results are obtained for those eddy-viscosity models (WALE and S3QR) that have the proper near-wall behavior, *i.e.* $\nu_e = O(y^3)$. To emphasize the benefits of LES modeling, the approximate computational cost of the simulations is displayed in the top horizontal axis of Figure 4 (left): it was measured on the MareNostrum 4 supercomputer and corresponds to a total integration period of 500 time-units. Finally, to see the effect of eddy-viscosity models in more detail, results for the average turbulent kinetic energy are shown in Figure 4 (right) for two meshes and two eddy-viscosity models (WALE and S3QR). All these results seem to confirm the suitability of the eddy-viscosity assumption for buoyancy-driven flows. For more details the reader is referred to [9]. Our future research plans include the extension of this analysis to higher Ra and testing *a posteriori* the new non-linear SGS heat flux models for air-filled RBC at Ra up to 10^{11} [10]. Prior to that, we aim to properly discretize tensorial eddy-diffusivity models. A first approximation to this problem is presented below.

4 ON THE PROPER DISCRETIZATION OF A TENSORIAL EDDY-DIFFUSIVITY MODEL

This section is devoted to the discretization of a tensorial eddy-diffusivity model, *i.e.*

$$\nabla \cdot q \approx \nabla \cdot \left(\mathsf{A} \nabla \overline{T}\right). \tag{12}$$

Notice that all the tensorial models presented in this work, including the already existing ones, fall in this template. We aim to preserve fundamental physical and mathematical properties when discretizing Eq.(12) where A is a 3×3 real-valued tensor (2×2 for 2D flows). Namely, the first property denoted as **Property P1** is the conservation of zero-th order moment (integral) of $\overline{T}$,

$$\int_\Omega \nabla \cdot (\mathsf{A} \nabla \overline{T}) dV = \int_{\partial\Omega} (\mathsf{A} \nabla \overline{T}) \cdot n dS = 0 \qquad \text{(no contribution from boundary } \partial\Omega\text{)}. \tag{13}$$

The second property [**Property P2**] is the symmetry preservation: Eq.(12) represents a diffusive operator (no interscale interaction). Hence, $\nabla \cdot \mathsf{A} \nabla$ is a symmetric operator if tensor A is symmetric ($\mathsf{A} = \mathsf{A}^T$),

$$< \psi, \nabla \cdot (\mathsf{A} \nabla \theta) > = - < \nabla \psi, \mathsf{A} \nabla \theta > \overset{\mathsf{A}=\mathsf{A}^T}{=} - < \mathsf{A} \nabla \psi, \nabla \theta > = < \nabla \cdot (\mathsf{A} \nabla \psi), \theta >, \tag{14}$$

where $< a, b > = \int_\Omega abdV$ is the usual inner-product of functions. Notice that the gradient is the adjoint of minus the divergence operator (and vice versa) provided that contributions from boundary, $\partial\Omega$, cancel, *i.e.* $\int_\Omega \nabla \cdot (ab) dV = < a, \nabla b > + < \nabla \cdot a, b > = \int_{\partial\Omega} ab \cdot n dS = 0$. The third property [**Property P3**] is the definiteness preservation; that is, given a positive (or negative) definite tensor, A, then the operator $\nabla \cdot \mathsf{A} \nabla$ is negative (or positive) semi-definite,

$$< \nabla \cdot (\mathsf{A} \nabla \theta), \theta > = - < \mathsf{A} \nabla \theta, \nabla \theta > \overset{\mathsf{A}=\mathsf{L}\mathsf{L}^T}{=} - < \mathsf{L} \nabla \theta, \mathsf{L} \nabla \theta > = - ||\mathsf{L} \nabla \theta||^2 \leq 0, \tag{15}$$

where the Cholesky decomposition of tensor A, $\mathsf{A} = \mathsf{L}\mathsf{L}^T$, assumes that A is a symmetric positive definite tensor. For negative definite tensors, $\mathsf{A} = -\mathsf{L}\mathsf{L}^T$, leading to the conclusion that $\nabla \cdot \mathsf{A} \nabla$ is then positive semi-definite. Two more properties of numerical nature can be added to the list. Namely, [**Property P4**] states that it is preferable to build up discretizations that are entirely based on already existing discrete operators in a standard CFD code. This obviously facilitates the implementation and the verification of the method. Finally, it is also desirable to naturally recover the numerical result obtained for an isotropic diffusive term, *i.e.* $\mathsf{A} = \kappa \mathsf{I}$. This last property will be referred as [**Property P5**].

First property **P1** relies on the Gauss theorem. Thus, Eq.(12) must be the discretized in divergence form,

$$\mathsf{M} q_s \in \mathbb{R}^n, \tag{16}$$

where $\mathsf{M} \in \mathbb{R}^{n \times m}$ represents the divergence operator in integral form, n and m are respectively the number of control volumes and faces on the computational domain, and $q_s \in \mathbb{R}^m$ is a discrete vector that contains the (turbulent) heat fluxes defined at the faces of the volumes. The subindices c and s refer to whether the variables are cell-centered or staggered at the faces. Otherwise stated, we follow the same notation used in Ref.[17]. Then, everything relies on the computation of q_s; therefore, hereafter we assume that

$$q_s = q_s(\mathsf{A}_c, T_c) \in \mathbb{R}^m, \tag{17}$$

where A_c is the cell-centered discrete counterpart of tensor A and T_c is the cell-centered discrete temperature field. Furthermore, we can assume that the following discrete operators are already available:

the discrete gradient operator, $\mathsf{G} \in \mathbb{R}^{m\times n}$, diagonal matrices containing the staggered, $\Omega_s \in \mathbb{R}^{m\times m}$, and cell-centered, $\Omega_c \in \mathbb{R}^{n\times n}$, control volumes and a cell-to-face interpolator, $\Pi_{c\to s} \in \mathbb{R}^{m\times n}$. To simplify the analysis we consider a 2D Cartesian mesh (extension to 3D is straightforward). In this case,

$$\mathsf{G} = \begin{pmatrix} \mathsf{G}_x \\ \mathsf{G}_y \end{pmatrix} \quad \text{and} \quad \Gamma_{c\to s} = \begin{pmatrix} \Pi_{c\to x} \\ \Pi_{c\to y} \end{pmatrix}, \tag{18}$$

where $\mathsf{G}_x \in \mathbb{R}^{m_x\times n}$ ($\mathsf{G}_y \in \mathbb{R}^{m_y\times n}$) represents the part of the discrete gradient operator, G, that computes the gradient at the m_x (m_y) faces staggered in the x (y) direction. The cell-to-face interpolator, $\Pi_{c\to s}$, is split in the same way: $\Pi_{c\to x} \in \mathbb{R}^{m_x\times n}$ and $\Pi_{c\to y} \in \mathbb{R}^{m_y\times n}$. Then, the discrete fluxes, q_s, can be approximated as follows

$$q_s \approx \begin{pmatrix} \Pi_{c\to x}\mathsf{A}_c^{xx}\Pi_{x\to c} & \Pi_{c\to x}\mathsf{A}_c^{xy}\Pi_{y\to c} \\ \Pi_{c\to y}\mathsf{A}_c^{xy}\Pi_{x\to c} & \Pi_{c\to y}\mathsf{A}_c^{yy}\Pi_{y\to c} \end{pmatrix} \begin{pmatrix} \mathsf{G}_x \\ \mathsf{G}_y \end{pmatrix} T_c, \tag{19}$$

where $\mathsf{A}_c^{xx} \in \mathbb{R}^{n\times n}$, $\mathsf{A}_c^{xy} \in \mathbb{R}^{n\times n}$ and $\mathsf{A}_c^{yy} \in \mathbb{R}^{n\times n}$ are diagonal matrices containing the cell-centered components of the symmetric tensor A. Previous expression can be written more compactly as

$$q_s \approx \tilde{\Pi}_{c\to s}\tilde{\mathsf{A}}_c\tilde{\Pi}_{s\to c}\mathsf{G}T_c, \tag{20}$$

where $\tilde{\Pi}_{c\to s}$, $\tilde{\mathsf{A}}_c$ and $\tilde{\Pi}_{s\to c}$ are block matrices given by

$$\tilde{\Pi}_{c\to s} = \begin{pmatrix} \Pi_{c\to x} & 0 \\ 0 & \Pi_{c\to y} \end{pmatrix} \quad \tilde{\mathsf{A}}_c = \begin{pmatrix} \mathsf{A}_c^{xx} & \mathsf{A}_c^{xy} \\ \mathsf{A}_c^{xy} & \mathsf{A}_c^{yy} \end{pmatrix} \quad \tilde{\Pi}_{s\to c} = \begin{pmatrix} \Pi_{x\to c} & 0 \\ 0 & \Pi_{y\to c} \end{pmatrix}. \tag{21}$$

At this point, we can investigate the restrictions imposed by property **P2** (symmetry preservation). Plugging previous expression into Eq.(16) leads to

$$\mathsf{M}q_s = \mathsf{M}\tilde{\Pi}_{c\to s}\tilde{\mathsf{A}}_c\tilde{\Pi}_{s\to c}\mathsf{G}T_c = \tilde{\mathsf{D}}_c T_c, \tag{22}$$

where $\tilde{\mathsf{D}}_c = \mathsf{M}\tilde{\Pi}_{c\to s}\tilde{\mathsf{A}}_c\tilde{\Pi}_{s\to c}\mathsf{G}$. Hence, this matrix must be symmetric, *i.e.*

$$\tilde{\mathsf{D}}_c = \tilde{\mathsf{D}}_c^T. \tag{23}$$

The above-mentioned duality between the gradient and divergence operator is translated into discrete level as follows (see Refs. [17, 18] for details)

$$\mathsf{G} = -\Omega_s^{-1}\mathsf{M}^T. \tag{24}$$

Then, plugging this into the definition of $\tilde{\mathsf{D}}_c$ leads to

$$\tilde{\mathsf{D}}_c = -\mathsf{M}\tilde{\Pi}_{c\to s}\tilde{\mathsf{A}}_c\tilde{\Pi}_{s\to c}\Omega_s^{-1}\mathsf{M}^T. \tag{25}$$

Recalling that matrix $\tilde{\mathsf{A}}_c$ is symmetric, then the symmetry of $\tilde{\mathsf{D}}_c$ is obtained by imposing the following relationship between the face-to-cell and the cell-to-face interpolators

$$\tilde{\Pi}_{s\to c} \equiv \Omega^{-1}\tilde{\Pi}_{c\to s}^T\Omega_s, \tag{26}$$

where $\Omega = \mathsf{I}_2 \otimes \Omega_c$ (for 2D) and $\Omega = \mathsf{I}_3 \otimes \Omega_c$ (for 3D) where $\mathsf{I}_2 \in \mathbb{R}^{2\times 2}$ and $\mathsf{I}_3 \in \mathbb{R}^{3\times 3}$ are identity matrices. This leads to

$$\tilde{\mathsf{D}}_c = -\mathsf{M}\tilde{\Pi}_{c\to s}\tilde{\mathsf{A}}_c\Omega^{-1}\tilde{\Pi}_{c\to s}^T\mathsf{M}^T. \tag{27}$$

In this way, both properties **P2** and **P3** are satisfied.

At this point, it worth paying some attention to the relation between the interpolation operators given in Eq.(26). A very similar relationship was already found (see Eq.22 in Ref. [17]), although in that case the interpolators were targeted for the cell-centered (and staggered) discrete velocity fields and, therefore, they included the projections onto the face-normal directions. Here, they are just interpolating a scalar field from face to cells, $\tilde{\Pi}_{s\to c}$ and vice versa, $\tilde{\Pi}_{c\to s}$. Taking the transpose of Eq.(26) and re-arranging terms, we can easily obtain an expression for $\tilde{\Pi}_{c\to s}$ in terms of $\tilde{\Pi}_{s\to c}$,

$$\tilde{\Pi}_{c\to s} \equiv \Omega_s^{-1}\tilde{\Pi}_{s\to c}^T\Omega. \tag{28}$$

Firstly, these relationships suggest that interpolations must be volume-weighted, but still there is some degree of freedom to define them. In Ref.[17], cell-to-face interpolation, $\tilde{\Pi}_{c\to s}$, was chosen with weights equal to $1/2$ for both adjacent discrete variables. This un-weighted interpolation follows straightforwardly by imposing the skew-symmetry of the discrete convective operator for second-order discretizations [18, 19, 17]. However, using this type of interpolation is probably not appropriate, except of course for the convective term, since in some cases may lead to instabilities in the context of the Fractional Step Method for collocated meshes [20]. The root of these issues is that variables of different nature are being interpolated. For instance, conservation of integral (volume-weighted) physical quantities (*e.g.* momentum, internal energy,...) is intimately tied up with metric preservation. Namely, the integral of the components in the x-direction (same analysis can be done for other spatial directions) of a staggered, $\phi_s \in \mathbb{R}^m$, and collocated, $\phi_c \in \mathbb{R}^{dn}$, fields can be respectively evaluated as

$$1_s^T\Omega_s\mathsf{N}_{s,x}\phi_s \in \mathbb{R} \quad \text{and} \quad 1_{c,x}^T\Omega\phi_c \in \mathbb{R}, \tag{29}$$

where $1_s \in \mathbb{R}^m$ is a column vector with ones located at the faces and $1_{c,x} \in \mathbb{R}^{dm}$ is a column vector with ones located at the cells corresponding to the x-direction (and zeros otherwise) where d is the number of dimensions ($d=2$ for 2D and $d=3$ for 3D). $\mathsf{N}_{s,x} \in \mathbb{R}^{m\times m}$ is a diagonal matrix containing the x-spatial components of the face normal vectors. Hence, $\Omega_s\mathsf{N}_{s,x}\phi_s$ can be interpreted as a column vector containing the scalar field ϕ_s integrated in the control volumes staggered in the x-direction. Then, left-multiplying this by 1_s, sums up all the control volumes. To study the effect of the face-to-cell interpolation, $\tilde{\Pi}_{s\to c}$, we take the vector defined at the faces, $\mathsf{N}_{s,x}\phi_s$, and we interpolate it to the cells where it can be integrated using the metric of the cells, Ω,

$$1_c^T\Omega\tilde{\Pi}_{s\to c}\mathsf{N}_{s,x}\phi_s \overset{(26)}{=} 1_c^T\tilde{\Pi}_{c\to s}^T\Omega_s\mathsf{N}_{s,x}\phi_s = (\tilde{\Pi}_{c\to s}1_c)^T\Omega_s\mathsf{N}_{s,x}\phi_s. \tag{30}$$

The same analysis can be done to study the effect of the cell-to-face interpolation, $\tilde{\Pi}_{c\to s}$. In this case, we take the vector defined at the cells, ϕ_c, and we interpolate it to the faces where it can be integrated using the metric of the faces, Ω_s,

$$1_s^T\mathsf{N}_{s,x}\Omega_s\tilde{\Pi}_{c\to s}\phi_c \overset{(28)}{=} 1_s^T\mathsf{N}_{s,x}\tilde{\Pi}_{s\to c}^T\Omega\phi_c \overset{\mathsf{N}_{s,x}=\mathsf{N}_{s,x}^T}{=} (\tilde{\Pi}_{s\to c}\mathsf{N}_{s,x}1_s)^T\Omega\phi_c. \tag{31}$$

Hence, comparing expressions (30) and (31) with those given in Eq.(29) it becomes clear that volume-weighted integrals will be respectively preserved if

$$\tilde{\Pi}_{c\to s}1_c = 1_s, \tag{32}$$

$$\tilde{\Pi}_{s\to c}\mathsf{N}_{s,x}1_s = 1_{c,x}. \tag{33}$$

The former implies that the face-to-cell interpolation, $\tilde{\Pi}_{s\to c}$, would preserve volume integrals (see Eq.30) whereas the latter implies that cell-to-face interpolation, $\tilde{\Pi}_{c\to s}$, would preserve volume integrals (see Eq.31). Unfortunately, only for uniform meshes both identities can be simultaneously satisfied since $\tilde{\Pi}_{c\to s}$ and $\tilde{\Pi}_{s\to c}$ are linked via Eq.(26); therefore, we have to choose. As mentioned above, in Ref. [17] we adopted an un-weighted interpolation for $\tilde{\Pi}_{c\to s}$; however, in view of this analysis, it seems more appropriate to use an un-weighted interpolation for $\tilde{\Pi}_{s\to c}$ leading to proper conservation of integral quantities defined at the cells (see Eq. 31).

In sum, the discretization of a tensorial eddy-diffusivity model given in Eq.(12) has been proposed in Eq.(27). Hereafter this method will be named as **Method D1**. By construction, this method satisfies all the properties (**P1-P4**) except **P5**, *i.e.* due to the additional interpolations, $\tilde{\Pi}_{c\to s}$ and $\tilde{\Pi}_{s\to c}$, it does not recover the numerical solution obtained for isotropic diffusivity, *i.e.* $\mathsf{A}=\kappa\mathsf{I}$. This forces to redefine Eq.(19) and the subsequent definitions. Namely,

$$q_s \approx \begin{pmatrix} \mathsf{A}_s^{xx} & \Pi_{c\to x}\mathsf{A}_c^{xy}\Pi_{y\to c} \\ \Pi_{c\to y}\mathsf{A}_c^{xy}\Pi_{x\to c} & \mathsf{A}_s^{yy} \end{pmatrix} \begin{pmatrix} \mathsf{G}_x \\ \mathsf{G}_y \end{pmatrix} T_c, \tag{34}$$

where $\mathsf{A}_s^{xx}=\mathrm{diag}(\Pi_{c\to x}\,\mathrm{diag}(\mathsf{A}_c^{xx}))$ and $\mathsf{A}_s^{yy}=\mathrm{diag}(\Pi_{c\to y}\,\mathrm{diag}(\mathsf{A}_c^{yy}))$. In this way, we avoid unnecessary interpolations for the coefficients of the diagonal matrices A_c^{xx} and A_c^{yy}. Moreover, we naturally preserve the same discretization for the isotropic case and, therefore, all properties (**P1-P5**) are preserved. This second method is referred as **Method D2**.

In summary, two discretization methods have been proposed:

$$q_s^{\mathbf{D1}} = \tilde{\mathsf{A}}_s^{\mathbf{D1}}\mathsf{G}T \qquad \text{where} \quad \tilde{\mathsf{A}}_s^{\mathbf{D1}} = \tilde{\Pi}_{c\to s}\tilde{\mathsf{A}}_c\tilde{\Pi}_{s\to c}, \tag{35}$$

$$q_s^{\mathbf{D2}} = \tilde{\mathsf{A}}_s^{\mathbf{D2}}\mathsf{G}T \qquad \text{where} \quad \tilde{\mathsf{A}}_s^{\mathbf{D2}} = \tilde{\Pi}_{c\to s}\tilde{\mathsf{A}}_c^{off}\tilde{\Pi}_{s\to c} + \mathrm{diag}(\tilde{\Pi}_{c\to s}\,\mathrm{diag}(\tilde{\mathsf{A}}_c)), \tag{36}$$

where $\tilde{\mathsf{A}}_c^{off}$ represents the off-diagonal elements of $\tilde{\mathsf{A}}_c$ given in Eq.(21). Hence, the only difference between method **D2** and **D1** is the treatment of the diagonal terms, *i.e.* $\tilde{\mathsf{A}}_s^{\mathbf{D1}}-\tilde{\mathsf{A}}_s^{\mathbf{D2}}$ is a diagonal matrix. As a final remark, although both methods have the same order of accuracy, which will depend on the order of accuracy of the underlying discretization method to construct basic discrete operators, the constant in front of the leading term in the local truncation error is lower for the method **D2**.

5 CONCLUDING REMARKS AND FUTURE RESEARCH

Nowadays, most of the CFD codes rely on the eddy-diffusivity assumption, $q^{eddy}\propto\nabla\overline{T}$, to model the SGS heat flux for LES simulations. Researchers' experience carrying out LES simulations of buoyancy-driven turbulence using this approach is, in general, quite frustrating. Namely, in many cases there is no relevant improvement compared with the results obtained without any SGS model. In other cases, the apparent improvement is simply due to the fact that the SGS model stabilizes the numerical simulation that otherwise (without model) would just blow up. The latter issue can be solved using numerical discretizations that are stable *per se* [17, 18, 19]. In any case, very small improvements are actually observed [1] leading to the necessity to use very fine grids (sometimes similar to DNS) to obtain reliable solutions. Furthermore, *a priori* analysis using DNS data of RBC at high Ra-numbers clearly shows that the classical (linear) eddy-diffusivity assumption is completely misaligned with the actual SGS heat flux.

In this context, we have firstly studied and confirmed the suitability of the eddy-viscosity assumption for buoyancy-driven turbulent flows. To do so, we have carried out *a posteriori* tests for different LES models at very low Prandtl numbers (liquid sodium, $Pr = 0.005$). Then, in the quest for more accurate models, we have proposed a new family of tensorial SGS heat flux models. Among all the possible candidates, we have chosen the so-called S2PR model given in Eq.(10) with $C_{s2pr} \approx 12.02$ [9]: it shows a very good representation of the SGS heat flux both in direction and magnitude. Moreover, apart from fulfilling a set of desirable properties (locality, Galilean invariance, numerical stability, proper near-wall behavior, and automatically switch-off for laminar and 2D flows), the proposed model is well-conditioned, and has a low computational cost and no intrinsic limitations for statistically in-homogeneous flows. Hence, it seems to be well suited for engineering applications. In this regard, the proper calculation of the subgrid characteristic length on unstructured grids [21] or the (dynamic?) determination of model constant are relevant issues that may affect the performance. Apart from this, our future research plans include the extension of this analysis to higher *Ra*-numbers and testing *a posteriori* the new tensorial SGS heat flux model for air-filled RBC problems at *Ra* up to 10^{11}. Prior to that, we also aim to properly discretize tensorial eddy-diffusivity models. A first approximation to this problem has been addressed in this paper.

ACKNOWLEDGMENTS

F.X.T., F.D. and A.O. have been financially supported by the *Ministerio de Economía y Competitividad*, Spain, ANUMESOL project (ENE2017-88697-R). F.X.T. and A.O. are supported by the Generalitat de Catalunya RIS3CAT-FEDER, FusionCAT project (001-P-001722). F.D. is supported by the Austrian Federal Ministry for Digital and Economic Affairs, the National Foundation for Research, Technology and Development, and the K1MET center for metallurgical research in Austria (www.k1-met.com). D.S. is supported by an FI AGAUR-Generalitat de Catalunya fellowship (2020FI B 00839). Calculations have been performed on the IBM MareNostrum 4 supercomputer at the BSC (PRACE 15th Call, Ref. 2016163972, "Exploring new frontiers in Rayleigh-Bénard convection" and Tier-1 RES projects IM-2020-2-0029 & IM-2020-3-0030 "Direct and Large-Eddy Simulation of buoyancy-driven turbulence in liquid metals"). The authors thankfully acknowledge these institutions.

REFERENCES

[1] F. Dabbagh, F. X. Trias, A. Gorobets, and A. Oliva, "A priori study of subgrid-scale features in turbulent Rayleigh-Bénard convection," *Physics of Fluids*, vol. 29, p. 105103, 2017.

[2] C. W. Higgins, M. B. Parlange, and C. Meneveau, "The heat flux and the temperature gradient in the lower atmosphere," *Geophysical Research Letter*, vol. 31, p. L22105, 2004.

[3] S. G. Chumakov, ""*A priori* study of subgrid-scale flux of a passive scalar in isotropic homogeneous turbulence," *Physical Review E*, vol. 78, p. 036313, 2008.

[4] A. Leonard, "Large-eddy simulation of chaotic convection and beyond," *AIAA paper*, vol. 97-0304, 1997.

[5] F. Dabbagh, F. X. Trias, A. Gorobets, and A. Oliva, "On the evolution of flow topology in turbulent Rayleigh-Bénard convection," *Physics of Fluids*, vol. 28, p. 115105, 2016.

[6] B. J. Daly and F. H. Harlow, "Transport equations in turbulence," *Physics of Fluids*, vol. 13, p. 2634,

1970.

[7] S. Peng and L. Davidson, "On a subgrid-scale heat flux model for large eddy simulation of turbulent thermal flow," *International Journal of Heat and Mass Transfer*, vol. 45, pp. 1393–1405, 2002.

[8] L. Engelmann, M. Klein, and A. M. Kempf, "A-posteriori LES assessment of subgrid-scale closures for bounded passive scalars," *Computers & Fluids*, vol. 218, p. 104840, 2021.

[9] F. X. Trias, F. Dabbagh, A. Gorobets, and C. Oliet, "On a proper tensor-diffusivity model for large-eddy simulation of buoyancy-driven turbulence," *Flow, Turbulence and Combustion*, vol. 105, pp. 393–414, 2020.

[10] F. Dabbagh, F. X. Trias, A. Gorobets, and A. Oliva, "Flow topology dynamics in a three-dimensional phase space for turbulent Rayleigh-Bénard convection," *Physical Review Fluids*, vol. 5, p. 024603, 2020.

[11] R. A. Clark, J. H. Ferziger, and W. C. Reynolds, "Evaluation of subgrid-scale models using an accurately simulated turbulent flow," *Journal Fluid Mechanics*, vol. 91, pp. 1–16, 1979.

[12] P. Sagaut, *Large Eddy Simulation for Incompressible Flows: An Introduction*. Springer, third ed., 2005.

[13] F. Nicoud and F. Ducros, "Subgrid-scale stress modelling based on the square of the velocity gradient tensor," *Flow, Turbulence and Combustion*, vol. 62, no. 3, pp. 183–200, 1999.

[14] A. W. Vreman, "An eddy-viscosity subgrid-scale model for turbulent shear flow: Algebraic theory and applications," *Physics of Fluids*, vol. 16, no. 10, pp. 3670–3681, 2004.

[15] R. Verstappen, "When does eddy viscosity damp subfilter scales sufficiently?," *Journal of Scientific Computing*, vol. 49, no. 1, pp. 94–110, 2011.

[16] F. X. Trias, D. Folch, A. Gorobets, and A. Oliva, "Building proper invariants for eddy-viscosity subgrid-scale models," *Physics of Fluids*, vol. 27, no. 6, p. 065103, 2015.

[17] F. X. Trias, O. Lehmkuhl, A. Oliva, C.D. Pérez-Segarra, and R.W.C.P. Verstappen, "Symmetry-preserving discretization of Navier-Stokes equations on collocated unstructured meshes," *Journal of Computational Physics*, vol. 258, pp. 246–267, 2014.

[18] R. W. C. P. Verstappen and A. E. P. Veldman, "Symmetry-Preserving Discretization of Turbulent Flow," *Journal of Computational Physics*, vol. 187, pp. 343–368, 2003.

[19] Y. Morinishi, T. Lund, O. Vasilyev, and P. Moin, "Fully Conservative Higher Order Finite Difference Schemes for Incompressible Flow," *Journal of Computational Physics*, vol. 143, pp. 90–124, 1998.

[20] D. Santos, J. Muela, N. Valle, and F. X. Trias, "On the interpolation problem for the Poisson equation on collocated meshes," in *14th World Congress in Computational Mechanics and ECCOMAS Congress (WCCM-ECCOMAS 2020)*, (Paris, France (online)), July 2020 (postponed to January 2021 due to COVID19 pandemic).

[21] F. X. Trias, A. Gorobets, M. H. Silvis, R. W. C. P. Verstappen, and A. Oliva, "A new subgrid characteristic length for turbulence simulations on anisotropic grids," *Physics of Fluids*, vol. 26, p. 115109, 2017.